

Open thermal cloak based on active thermal metasurfaces

Bao-Quan Hou(侯宝泉), Fei Sun(孙非), Yi-Chao Liu(刘一超), Jia-Peng Wang(王嘉鹏), Ya-Ru Feng(冯亚茹), Bin-Zhao Cao(曹斌照), Hong-Ming Fei(费宏明), and Jie Wu(武洁)
Citation: Chin. Phys. B, 2026, 35 (**5**): 054401. DOI: 10.1088/1674-1056/ae48bf
http://cpb.iphy.ac.cn; http://iopscience.iop.org/cpb

What follows is a list of articles you may be interested in

Thermal diode with switchable cloaking effect enabled by asymmetric temperature-dependent thermal conductivity

Mengzhen Xue(薛梦贞), Jun Wang(王军), and Guodong Xia(夏国栋)
Chin. Phys. B, 2025, 34 (**11**): 114403. DOI: 10.1088/1674-1056/ae118b

Strain modulated phonon transport in one-dimensional nonlinear lattice with on-site potential

Hongbin Chen(陈宏斌), Nianbei Li(李念北), and Jie Chen(陈杰)
Chin. Phys. B, 2025, 34 (**11**): 114401. DOI: 10.1088/1674-1056/adf1ea

Normal energy and stretch diffusion in a one-dimensional momentum conserving lattice with nonlinear bounded kinetic energy

Hongbin Chen(陈宏斌), Qin-Yi Zhang(张钦奕), Jiahui Wang(王佳惠), Nianbei Li(李念北), and Jie Chen(陈杰)
Chin. Phys. B, 2025, 34 (**9**): 094401. DOI: 10.1088/1674-1056/addce5

General three-dimensional thermal illusion metamaterials

Tianfeng Liu(刘天丰), Zhaochen Wang(王兆宸), Zhan Zhu(朱展), and Run Hu(胡润)
Chin. Phys. B, 2024, 33 (**4**): 044401. DOI: 10.1088/1674-1056/ad09aa

Construction and mechanism analysis on nanoscale thermal cloak by *in-situ* annealing silicon carbide film

Jian Zhang(张健), Hao-Chun Zhang(张昊春), Zi-Liang Huang(黄子亮), Wen-Bo Sun(孙文博), and Yi-Yi Li(李依依)
Chin. Phys. B, 2022, 31 (**1**): 014402. DOI: 10.1088/1674-1056/ac2809

Open thermal cloak based on active thermal metasurfaces

Bao-Quan Hou(侯宝泉)[1], Fei Sun(孙非)[1,†], Yi-Chao Liu(刘一超)[1], Jia-Peng Wang(王嘉鹏)[1], Ya-Ru Feng(冯亚茹)[1], Bin-Zhao Cao(曹斌照)[1], Hong-Ming Fei(费宏明)[1], and Jie Wu(武洁)[2]

[1] *Key Laboratory of Advanced Transducers and Intelligent Control System, Ministry of Education and Shanxi Province, College of Physics and Optoelectronics, Taiyuan University of Technology, Taiyuan* 030024, *China*
[2] *Taiyuan University, Taiyuan* 030000, *China*

(Received 17 December 2025; revised manuscript received 4 February 2026; accepted manuscript online 23 February 2026)

The enclosed configuration of conventional thermal cloaks prevents the passage of matter across their boundaries. To overcome this limitation, we propose an open thermal cloak (OTC) that simultaneously provides effective thermal cloaking and incorporates a functional exit that allows unimpeded passage and exchange of matter. The OTC integrates a closed thermal cloak with an exit (CTCE) and a thermal shifter designed via coordinate transformation. The thermal shifter compensates for performance degradation caused by the exit by transferring the thermal regulation function of the removed segment back to the exit location, using a material with equivalent negative thermal conductivity derived from transformation thermotics. For practical implementation, this idealized material is replaced with discrete active thermal metasurfaces (ATMs) at the boundary to replicate the required heat flux conditions. Numerical simulations show that the ATM-based OTC exhibits excellent cloaking performance under varying heat flow directions and across exits of different sizes and shapes, maintaining background temperature field integrity and a near-uniform temperature distribution inside the protected region. The average temperature disturbance induced is significantly lower than that of CTCE and a directly exposed object, with performance approaching that of an ideal closed thermal cloak (CTC). This work breaks the enclosure limitation of traditional thermal cloaks and shows promise for infrared thermal protection of underground shelters and the thermal management of heat-sensitive electronics.

Keywords: thermal cloaking, thermal metasurface, transformation thermotics, open cloak, active metasurface

PACS: 44.10.+i, 44.90.+c, 81.05.Xj

DOI: 10.1088/1674-1056/ae48bf **CSTR:** 32038.14.CPB.ae48bf

1. Introduction

Thermal cloaking utilizes specialized thermal structures composed of materials with engineered thermal conductivity, known as thermal metamaterials/metasurfaces,[1–7] which guide heat flow around an object within a concealed region and allow it to continue along its original path.[8–12] This approach preserves the external background temperature field from disturbance while maintaining a near-zero temperature gradient inside the concealed region, thereby shielding the protected object from external thermal influence. After years of development, various thermal cloaking structures have been proposed for diverse applications, showing promise in areas such as infrared protection for underground shelters and thermal management of heat-sensitive electronic components.[13–15]

Thermal cloaking is primarily achieved through three design approaches. The first method employs transformation thermotics,[16–19] using coordinate transformation to create media that guide heat flow around the concealed region. These materials typically exhibit anisotropic and spatially graded thermal conductivity. The second approach involves designing multi-layer core-shell structures. By solving the steady-state heat conduction Laplace equation under the condition of an undisturbed background temperature field, the required relationships between thermal conductivity and geometric parameters for each layer are derived.[8–10,20–22] The third method utilizes optimization techniques such as topological optimization or artificial intelligence algorithms to directly determine material parameters that minimize disturbance to the background temperature field.[23–27] Recent advances in thermal metamaterials and metasurfaces have expanded thermal cloaking beyond single-physics (thermal) applications to multi-physical systems.[28–34] New developments also include functionally switchable thermal management structures,[33,35–40] and cloaking designs adaptable to arbitrary shapes.[23,41] Nevertheless, current thermal cloaking technology remains primarily focused on enclosed configurations, where the concealed object is completely encapsulated or continuously surrounded by a shell. In practical applications, however, there is often a need for matter exchange between the interior and exterior of the thermal cloak — such as in thermal shielding for on-chip electrically interconnected systems or open-configuration chemical reactors. So far, there has been almost no theoretical research or effective methods developed for open thermal cloaking structures.

As shown in Fig. 1(a), in a two-dimensional on-chip system, the presence of on-chip components causes thermal in-

[†]Corresponding author. E-mail: sunfei@tyut.edu.cn

© 2026 Chinese Physical Society and IOP Publishing Ltd. All rights, including for text and data mining, AI training, and similar technologies, are reserved.

terference in the background temperature distribution. These integrated components themselves also experience heat flow impact due to the background thermal flow, resulting in a non-zero temperature gradient inside them. As shown in Fig. 1(b), a classic CTC can be designed by solving the Laplace equations and wrapped around the original on-chip components to achieve a thermal cloaking effect: the background temperature distribution remains undisturbed, and the temperature inside the on-chip components becomes uniform (with a zero-temperature gradient, meaning no heat flow impact). However, considering many practical applications where on-chip integrated components require electrical connections or matter exchange with the external environment, it is necessary to remove a portion of the CTC from Fig. 1(b) to serve as an exit for internal matter or charge flow. To enable CTCE to still maintain good thermal cloaking functionality for its internal components, this study proposes placing a thermal shifter with heat translation capability, designed via folding transformation based on transformation thermotics,[15–18] around it. As shown in Fig. 1(c), if the material removed from the CTC (corresponding to the exit location) is placed at a specific position within the thermal shifter, the thermal regulation function lost due to the removed CTC part can be compensated back to the exit location via the thermal shifter. This compensates for the impact of introducing the exit on the original cloaking effect, thereby achieving a thermal cloaking functionality close to that in Fig. 1(b). Consequently, the structure formed by the combination of the thermal shifter and the CTCE is named the OTC. The OTC in Fig. 1(c) can simultaneously achieve effective thermal cloaking for the on-chip integrated components within its internal thermal protection zone, while enabling matter exchange between the thermal protection zone and the on-chip background environment (see the inset in Fig. 1(c)).

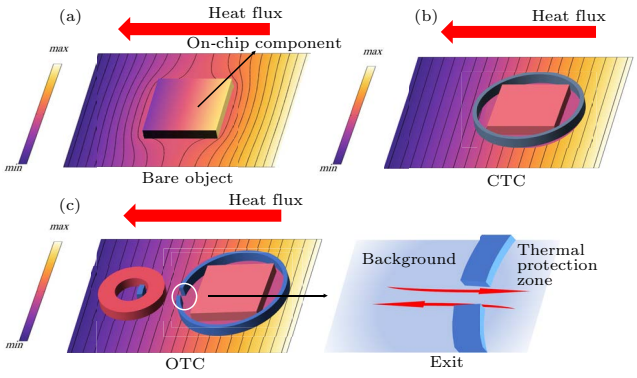


Fig. 1. (a) Heat flow directly impacts a bare on-chip component. (b) Heat flow impacts an on-chip component equipped with CTC. (c) Heat flow impacts an on-chip component equipped with OTC.

2. Theoretical design

The OTC is composed of two functional units: a CTCE and a thermal shifter. First, a CTC needs to be designed. By solving the steady-state heat conduction Laplace equation $\nabla \cdot (\kappa \nabla T) = 0$, the relationship between the thermal conductivity of each region in the CTC and the inner and outer radii can be derived (the detailed derivation is provided in supplementary note 1)

$$\left(\frac{R_1}{R_2}\right)^2 = \frac{(\kappa_1+\kappa_2)(\kappa_2-\kappa_3)}{(\kappa_2+\kappa_3)(\kappa_2-\kappa_1)}. \tag{1}$$

Here, R_1 and R_2 are the inner and outer radii of the CTC, respectively; κ_1, κ_2, and κ_3 are the thermal conductivities of the thermal protection zone, the cloak layer, and the background, respectively.

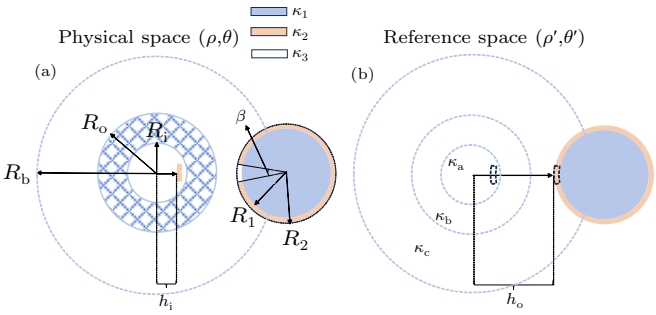


Fig. 2. Coordinate transformation between the physical space (a) and the reference space (b). The function of the thermal shifter (blue grid section) is to displace the thermal effect at point (h_i, 0) in the physical space (a) by a certain distance, transforming it to point (h_o, 0) in the reference space (b). The thermal shifter possesses an equivalent negative thermal conductivity.

In the reference space, the removed segment remains part of the cloak structure (Fig. 2(b)), while in the physical space it serves as a passage for matter exchange (Fig. 2(a)). The key challenge is thus designing a thermal shifter capable of transferring thermal effects from an internal point (h_i, 0) to an external spatial location (h_o, 0). As shown in Fig. 2(a), the annular thermal shifter, with inner radius R_i and outer radius R_o, and a transformation-defined boundary radius $R_b = R_o^2/R_i$, designed via transformation thermotics, exhibits equivalent negative thermal conductivity. With the center of the thermal shifter as the origin, the coordinate transformation between the physical space (ρ, θ, z) and the reference space (ρ', θ', z') can be expressed as

$$\begin{aligned}
(\rho',\theta',z') &= \left(\frac{R_b}{R_i}\rho,\ \theta,\ z\right), \text{ for region } \rho \le R_i,\\
(\rho',\theta',z') &= \left(\frac{R_o^2}{\rho},\ \theta,\ z\right), \text{ for region } R_i < \rho < R_o,\\
(\rho',\theta',z') &= (\rho,\theta,z), \text{ for region } \rho \ge R_o.
\end{aligned} \tag{2}$$

Based on the boundary condition requirements, the thermal conductivity is derived through transformation thermotics as

$$\kappa = \kappa_b \frac{\sqrt{g}}{\sqrt{\gamma}} \frac{J g^{-1} J^T \gamma}{\det(J)}, \tag{3}$$

where $\gamma = \mathrm{diag}(1, \rho'^2, 1)$, $g = \mathrm{diag}(1, \rho^2, 1)$, κ_b represents the thermal conductivity of the background material, and J denotes the Jacobian matrix. The Jacobian matrix J can be expressed as

$$\begin{aligned} J &= \mathrm{diag}\left\{\frac{R_\mathrm{i}}{R_\mathrm{b}}, 1, 1\right\}, \text{ for region } \rho \le R_\mathrm{i}, \\ J &= \mathrm{diag}\left\{-\frac{R_\mathrm{o}^2}{\rho'^2}, 1, 1\right\}, \text{ for region } R_\mathrm{i} \le \rho \le R_\mathrm{o}, \\ J &= \mathrm{diag}\{1, 1, 1\}, \text{ for region } \rho \ge R_\mathrm{o}. \end{aligned} \tag{4}$$

Then, the thermal conductivity in the physical space can be obtained as

$$\begin{aligned} \kappa &= \kappa_\mathrm{b}\mathrm{diag}\left\{1, 1, \frac{R_\mathrm{b}^2}{R_\mathrm{i}^2}\right\}, \text{ for region } \rho \le R_\mathrm{i}, \\ \kappa &= -\kappa_\mathrm{b}\mathrm{diag}\left\{1, 1, \frac{R_\mathrm{o}^4}{\rho^4}\right\}, \text{ for region } R_\mathrm{i} < \rho < R_\mathrm{o}, \\ \kappa &= \kappa_\mathrm{b}\mathrm{diag}\{1, 1, 1\}, \text{ for region } \rho \ge R_\mathrm{o}. \end{aligned} \tag{5}$$

If we only consider heat conduction in the two-dimensional ρ–θ plane, then the thermal conductivity in each region is isotropic and satisfies

$$\begin{aligned} \kappa &= \kappa_\mathrm{b}, \text{ for region } \rho \le R_\mathrm{i} \text{ or } \rho \ge R_\mathrm{o}, \\ \kappa &= -\kappa_\mathrm{b}, \text{ for region } R_\mathrm{i} < \rho < R_\mathrm{o}. \end{aligned} \tag{6}$$

This implies that the region $R_\mathrm{i} < \rho < R_\mathrm{o}$ is composed of an isotropic material with negative thermal conductivity, while the remaining regions consist of materials with positive thermal conductivity. From the coordinate transformation, we know $h_\mathrm{o} = h_\mathrm{i} \cdot R_\mathrm{b}/R_\mathrm{i}$, $R_\mathrm{b} = R_\mathrm{o}^2/R_\mathrm{i}$, and finally obtain

$$\frac{h_\mathrm{o}}{h_\mathrm{i}} = \left(\frac{R_\mathrm{o}}{R_\mathrm{i}}\right)^2. \tag{7}$$

The derived conductivity tensor ensures that a heat flow $\boldsymbol{q}$ at (h_i, 0) produces an identical heat flow $\boldsymbol{q}'$ at (h_o, 0). As a result, the thermal shifter restores the thermal-regulation function originally provided by the removed CTC segment.

3. Numerical simulation

Under uniform thermal excitation, the CTC maintains unbent background isotherms (Fig. 3(d)), confirming that heat flow bypasses the cloak undisturbed. Within its thermal protection zone, the heat flow direction aligns with the background (Fig. 3(a)) and exhibits a uniform magnitude (Fig. 3(g)). Introducing an exit within the CTC, however, curves the background isotherms (Fig. 3(e)), indicating disrupted heat flow. Inside the CTCE zone, the heat flow direction diverges from the background, the temperature distribution deviates significantly from that of the CTC (Fig. 3(b)), and the heat flow magnitude becomes non-uniform — particularly

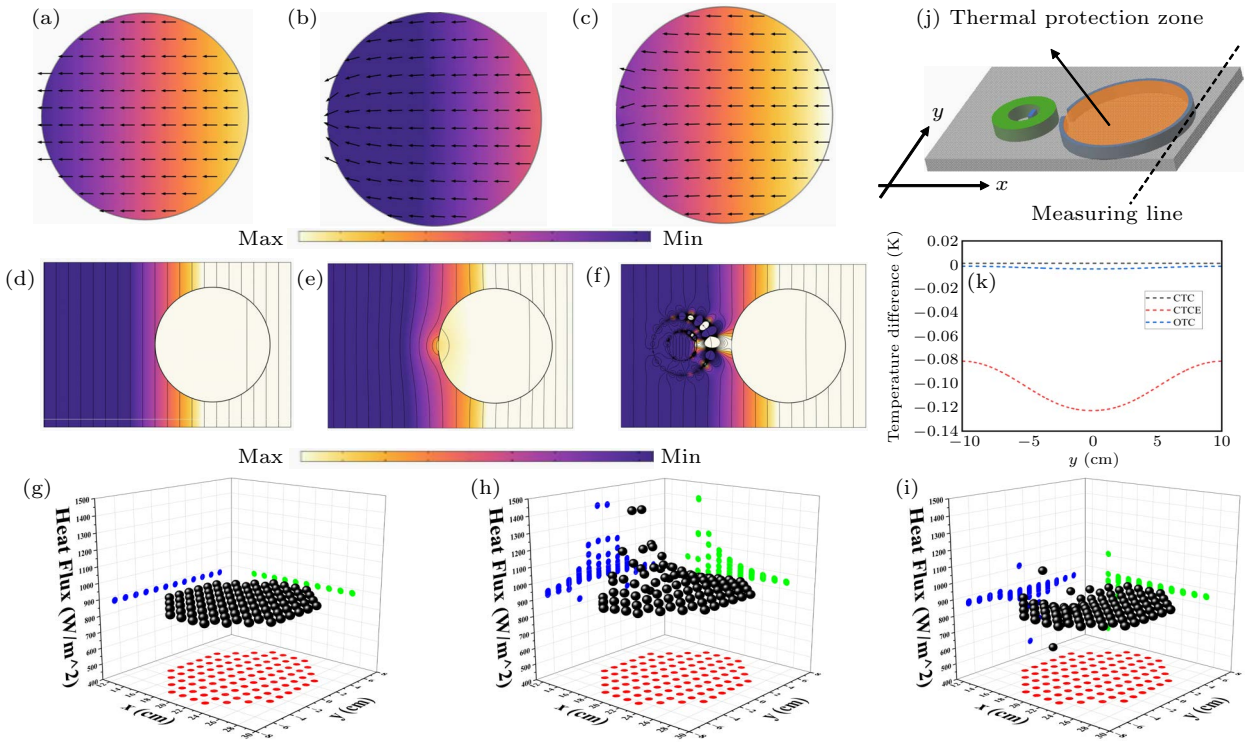


Fig. 3. Panels (a)–(c) respectively show the heat flow direction and temperature distribution (2D simulation) within the thermal protection zone of the CTC (a), CTCE (b), and OTC (c) when a heat flow is applied along the x-direction. Panels (d)–(f) display the temperature distribution (2D simulation) over the entire region for the CTC, CTCE, and OTC, respectively. Panels (g)–(i) show the heat flow intensity at different locations within the thermal protection zone of the CTC, CTCE, and OTC, respectively. Panel (j) illustrates the structure of the OTC. Panel (k) presents the distribution of the temperature difference from the ideal value at various positions along the measuring line for the CTC, CTCE, and OTC. The measuring line is a vertical line running through the top and bottom boundaries, parallel to the side boundaries, located 27.6 cm from the left boundary.

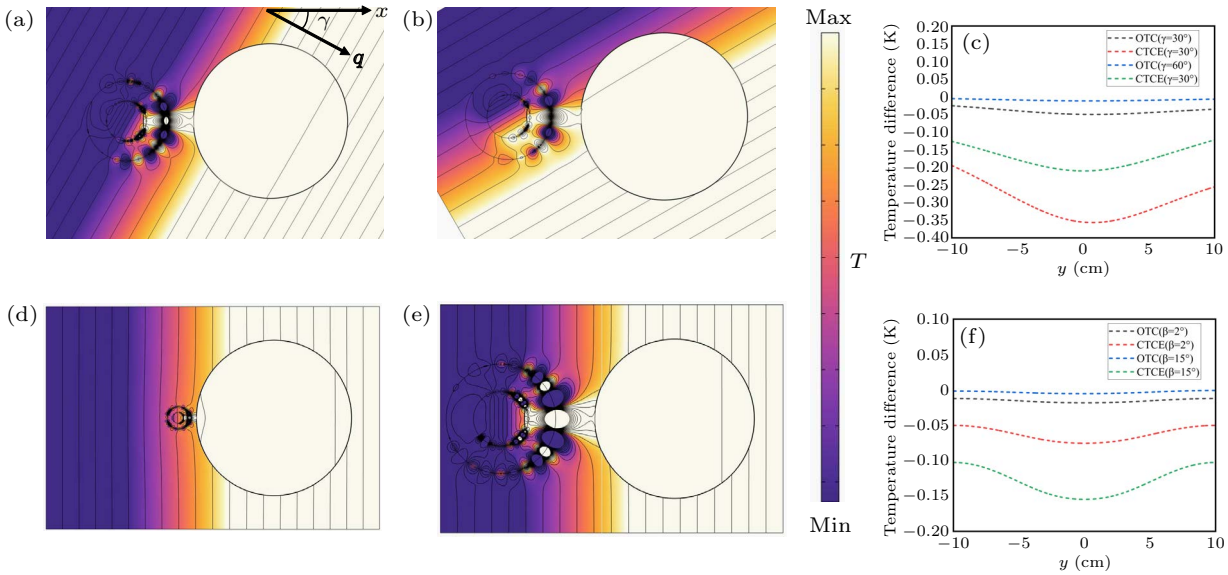


Fig. 4. Panels (a) and (b) show the temperature distributions (2D simulation) of the OTC when the heat flow is incident at angles of 30° and 60°, respectively. Panel (c) displays the temperature difference distribution curves from the ideal value along the measuring line for both the OTC and CTCE under 30° and 60° heat flow incidence. Panel (d) presents the temperature distribution (2D simulation) of the OTC utilizing a smaller thermal shifter designed for a smaller exit ($\beta = 2°$). Panel (e) shows the temperature distribution (2D simulation) of the OTC employing a larger thermal shifter to accommodate a larger exit ($\beta = 15°$). Panel (f) illustrates the distribution of the temperature difference from the ideal value along the measuring line for the OTC and CTCE with different exit angles.

elevated near the exit (Fig. 3(h)). In contrast, the OTC preserves straight background isotherms (Fig. 3(f)). Its internal heat flow direction closely matches the background, with the temperature distribution resembling that of the CTC (Fig. 3(c)) and a relatively uniform heat flow magnitude (Fig. 3(i)). Measurements along the measuring line (Fig. 3(j)) show that the OTC's average temperature disturbance is 10.2% of the CTCE's (Fig. 3(k)) and below 1.1% of the directly exposed object's, demonstrating excellent thermal cloaking performance (simulation parameters are detailed in supplementary note 2).

The OTC maintains excellent cloaking performance under varying heat flow directions (Figs. 4(a) and 4(b)). At 30° incidence, the average temperature disturbance along the measuring line is 0.04 K for the OTC versus 0.32 K for the CTCE; at 60°, it is 0.01 K for the OTC versus 0.19 K for the CTCE (Fig. 4(c)). Similarly, the OTC performs effectively across various exit angles β. For a larger exit ($\beta = 15°$), the average disturbance is 0.004 K (OTC) versus 0.14 K (CTCE). For a smaller exit ($\beta = 2°$), it is 0.015 K (OTC) versus 0.07 K (CTCE) (Figs. 4(c)–4(e)) (simulation details in supplementary note 2; other scenarios in supplementary note 3).

4. Realization design

To implement the OTC, we emulate equivalent negative thermal conductivity by using ATMs within a positive-conductivity background.[42,43] As illustrated in Fig. 5(a), embedding a region with conductivity $-\kappa_b$ in a background of κ_b results in reversed temperature gradients across the boundary — a hallmark of negative conductivity. By replacing this region with a positive-conductivity material and introducing boundary heat sources (Fig. 5(b)), the equivalent heat flux continuity can be maintained. The required boundary heat source density is given by $q_s = -2q_1 = -2\kappa_b \boldsymbol{u}\nabla T$, where $\boldsymbol{u}$ is the unit normal vector at the boundary. This enables the realization of negative thermal conductivity effects via active thermal control with ATMs. This approach effectively counteracts the reverse heat flow, reproducing the original temperature distribution.

For practical implementation, the continuous boundary heat source distribution is discretized into a finite number of line heat sources uniformly distributed along the boundary (Fig. 5(c)). This discretization can be regarded as a piecewise approximation of the continuous heat source density, where each discrete source represents the integrated heat power over a small angular segment $\Delta\theta$. When $\Delta\theta$ is sufficiently small, the discrete formulation converges to the continuous boundary condition. Accordingly, the power of the m-th line heat source located at angular position θ_m can be obtained by integrating the continuous heat source density over the corresponding angular interval, yielding

$$Q_m = \int_{\theta_m - \frac{\Delta\theta}{2}}^{\theta_m + \frac{\Delta\theta}{2}} q_s r \, \mathrm{d}\theta, \tag{8}$$

where θ_m is the angular position of the m-th source. By deploying discrete line heat sources along the boundary, the temperature control effect of negative thermal conductivity can be faithfully replicated within a positive-conductivity system.

Two-dimensional simulations confirm that the OTC based on ATMs, the active version using heat sources, achieves effective thermal cloaking (Figs. 5(d)–5(g)). Under x-directional heat flow at $\beta = 10°$, both continuous and discrete sources

yield low average temperature disturbances along the measuring line (0.014 K to 0.037 K) with small standard deviations in the thermal protection zone (0.281–0.288), significantly outperforming the CTCE (0.1244 K, 0.325). Figure 5(h) further shows that the OTC consistently induces lower disturbance than the CTCE along the measuring line (other details are in supplementary note 2).

For practical implementation, cloaking performance saturates with $m = 24$ and $n = 12$ discrete sources. Practically, the deployment of 36 heat sources is technically feasible. If deploying all 36 sources is constrained, an optimized non-uniform layout concentrating sources near the opening maintains effective cloaking by regulating the critical local thermal field (supplementary note 2). These sources can use semiconductor thermoelectric coolers (TECs), which serve as controllable local sources in thermal metasurfaces.[42–45] Modern TECs provide the high-power density and fast response needed for the precise, dynamic heat flux regulation required here,[46,47] supporting both layout schemes.

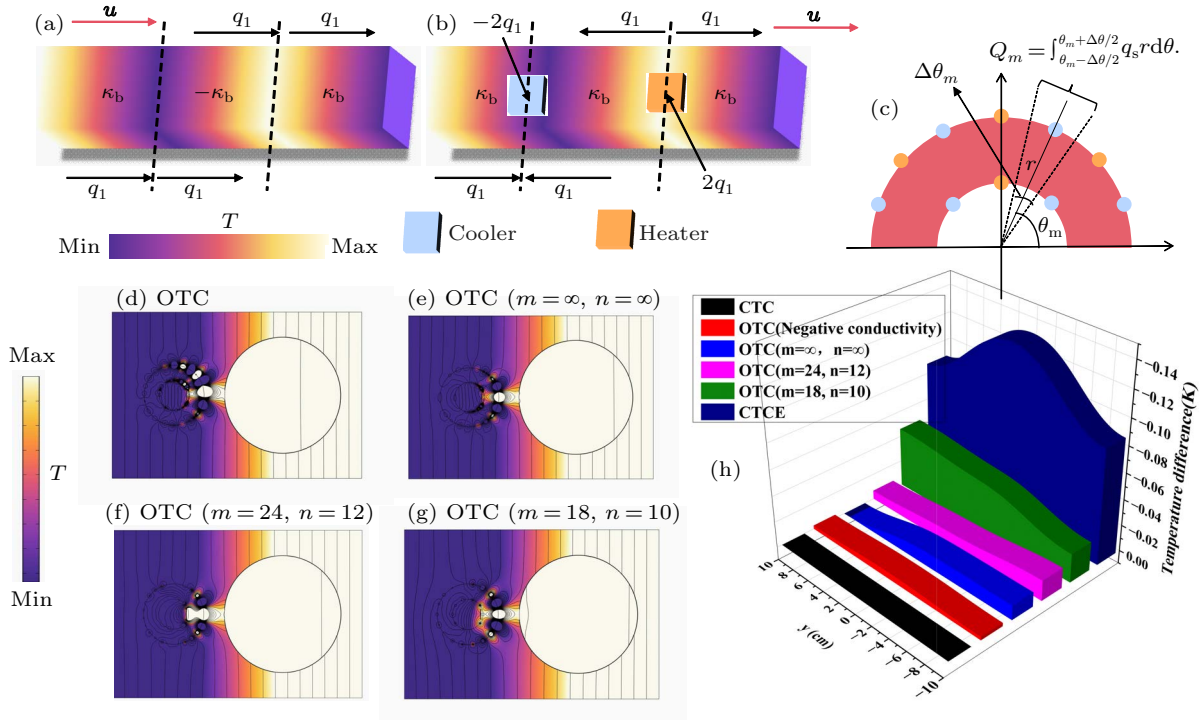


Fig. 5. (a) Temperature and heat flow with a negative thermal conductivity material embedded in a positive-conductivity background. (b) Same distribution achieved by replacing the negative-conductivity material with a positive-conductivity material and a configuration of coolers and heaters for active thermal control. (c) Power calculation method for discrete line heat sources in the thermal shifter. (d) OTC temperature distribution using negative thermal conductivity. (e) OTC temperature distribution with continuous boundary heat sources. (f) and (g) OTC temperature distributions using discrete boundary heat sources (m and n denote outer and inner source counts). (h) Temperature deviation along the measuring line for CTC, CTCE, and various OTC configurations.

This work improves upon traditional conduction-dominated enclosed thermal cloaks[8,10,11,18,28] to realize the OTC with a functional exit. In practical applications, however, material exchange through the exit may introduce convective heat transfer. The OTC remains effective under weak convection, but strong convection would require further integration with existing convective thermal metamaterials for enhanced performance.[48–51] Additionally, the active heat sources used for OTC functionality generate waste heat, which could create new infrared signatures. This can be addressed by incorporating infrared stealth metasurfaces,[52–54] guiding waste heat away through thermal conduits, or embedding the heat sources internally to minimize external thermal detection.

5. Conclusion

In summary, we realized an OTC for conduction-dominated scenarios by integrating a thermal shifter, designed via coordinate transformation, with the CTCE. Practical feasibility was achieved by employing discrete line heat sources at the boundary to mimic the heat flux of negative thermal conductivity material, thus enabling equivalent negative thermal conductivity. Numerical simulations confirm the OTC's excellent omnidirectional thermal cloaking performance. It supports large exits and permits using a smaller thermal shifter for smaller exits, saving space. This device shows strong application potential in infrared protection for underground shelters and thermal management of heat-sensitive electronic components.

Acknowledgments

This project was supported by the National Natural Science Foundation of China (Grant Nos. 12274317 and 12374277), the San Jin Talent Support Program — Shanxi Provincial Youth Top-notch Talent Project, the Natural Science Foundation of Shanxi Province (Grant No. 202303021211054), the Shanxi Province Higher Education Institutions Young Faculty Research and Innovation Support Program (Grant No. 2025Q006), and the College Student Innovation Project in Taiyuan University of Technology (Grant No. 20250164).

References

[1] Yang S, Wang J, Dai G L, Yang F B and Huang J P 2021 *Phys. Rep.* **908** 1
[2] Hu R, Xi W, Liu Y D, Tang K C, Song J L, Luo X B, Wu J Q and Qiu C W 2021 *Mater. Today* **45** 120
[3] Zhang Z R, Xu L J, Qu T, Lei M, Lin Z K, Ouyang X P, Jiang J H and Huang J P 2023 *Nat. Rev. Phys.* **5** 218
[4] Yang F B, Zhang Z, Xu L J, Liu J, Jin P, Zhuang P F, Lei M, Liu J R, Jiang J H, Ouyang X P, Marchesoni F and Huang J P 2024 *Rev. Mod. Phys.* **96** 015002
[5] Li Y, Li W, Han T, Zheng X, Li J X, Li B W, Fan S H and Qiu C W 2021 *Nat. Rev. Mater.* **6** 488
[6] Qiu Y G, Nomura M, Zhang Z W, *et al.* 2025 *Front. Phys.* **20** 065500
[7] Liu T F, Wang Z C, Zhu Z, Hu R 2024 *Chin. Phys. B* **33** 044401
[8] Schittny R, Kadic M, Guenneau S and Wegener M 2013 *Phys. Rev. Lett.* **110** 195901
[9] Xu H Y, Shi X H, Gao F, Sun H D and Zhang B L 2014 *Phys. Rev. Lett.* **112** 054301
[10] Han T C, Bai X, Gao D L, Thong J T L, Li B W and Qiu C W 2014 *Phys. Rev. Lett.* **112** 054302
[11] Hou Q W, Li J C and Zhao X P 2021 *Chin. Phys. Lett.* **38** 010503
[12] Sun R, Sun F and Liu Y C 2024 *Opto. Electron. Eng.* **51** 240191
[13] Narayana S and Sato Y 2012 *Phys. Rev. Lett.* **108** 214303
[14] Han T C, Bai X, Thong J T L, Li B W and Qiu C W 2014 *Adv. Mater.* **26** 1731
[15] Huang J P 2020 *Theoretical Thermotics* (Singapore: Springer)
[16] Xu L J and Huang J P 2023 *Transformation Thermotics and Extended Theories: Inside and Outside Metamaterials* (Singapore: Springer Nature)
[17] Guenneau S, Amra C and Veynante D 2012 *Opt. Express* **20** 8207
[18] Fan C Z, Gao Y and Huang J P 2008 *Appl. Phys. Lett.* **92** 251907
[19] Wu Y F, Wang B, Wu C L, Yao N Z, Wang H, Wang X S and Wang X S 2025 *Int. Commun. Heat Mass Transfer* **164** 108798
[20] Xu L J and Huang J P 2020 *Chin. Phys. Lett.* **37** 120501
[21] Shan Q R, Shao C R, Wang J and Xia G D 2023 *Chin. Phys. Lett.* **40** 104401
[22] Qin C L, Yang J J, Huang M and Hu Y Y 2014 *Acta Phys. Sin.* **63** 194402 (in Chinese)
[23] Wang Y H, Sha W, Xiao M, Qiu C W and Gao L 2023 *Adv. Mater.* **35** 2302387
[24] Chen J W, Yan Z M, Lin F H, Wang Y and Lu H R 2024 *Int. Commun. Heat Mass Transfer* **159** 107976
[25] Xu X Q, Gu X F D and Chen S K 2023 *Int. J. Heat Mass Transfer* **202** 123720
[26] Kato S, Takejima K, Song Z Q and Fujii G 2025 *Int. J. Heat Mass Transfer* **242** 126834
[27] Hirasawa K, Nakami I, Ooinoue T, Asaoka T and Fujii G 2022 *Int. J. Heat Mass Transfer* **194** 123093
[28] Ma Y G, Liu Y C, Raza M, Wang Y D and He S 2014 *Phys. Rev. Lett.* **113** 205501
[29] He S, Zhang R H and Liang J B 2024 *Opto-Electron. Adv.* **7** 240211
[30] Liu Y C, Chen H C, Zhao G and Sun F 2024 *iScience* **27** 110105
[31] Liu Y C, Ma X M, Chao K, Sun F, Chen Z H, Shan J Y, Chen H C, Zhao G and Chen S J 2024 *Opto. Electron. Sci.* **3** 230027
[32] Feng H L, Zhang X W, Zhou L M, Zhang Y K and Ni Y S 2024 *Chin. Phys. B* **33** 038102
[33] Lei M, Xu L J and Huang J P 2023 *Mater. Today Phys.* **34** 101057
[34] Sun F, Zhang H X, Liu Y C, Qin W Q and Li D Z 2025 *Small Struct.* **6** 202500352
[35] Li H G, Wang D, Xu G Q, Liu K P, Zhang T, Li J X, Tao G M, Yang S H, Lu Y H, Hu R, Lin S S, Li Y and Qiu C W 2024 *Nat. Commun.* **15** 2169
[36] Lou Q and Xia M G 2023 *Chin. Phys. Lett.* **40** 094401
[37] Li J X, Li Y, Cao P C, Yang T Z, Zhu X F, Wang W Y and Qiu C W 2020 *Adv. Mater.* **32** 2003823
[38] Guo J, Xu G Q, Tian D, Qu Z G and Qiu C W 2022 *Adv. Mater.* **34** 2201093
[39] Ju R, Cao P C, Wang D, Qi M H, Xu L J, Yang S H, Qiu C W, Chen H S and Li Y 2024 *Adv. Mater.* **36** 2309835
[40] Xue M Z, Wang J and Xia G D 2025 *Chin. Phys. B* **34** 114403
[41] Gao Y 2021 *Chin. Phys. Lett.* **38** 020501
[42] Liu Y C, Chao K, Sun F, Chen S J, Dai H T and Chen H C 2023 *Adv. Mater.* **35** 2210981
[43] Liu Y C, Qi Y W, Sun F, Shan J Y, Chen H C, Hao Y Y, Fei H M, Cao B Z, Liu X and Huo Z Z 2026 *Adv. Sci.* **13** e19386
[44] Liu Q, Wang Z C, Kim S K, Luo X B, Ben-Abdallah P, Choi W and Hu R 2025 *Mater. Today Phys.* **59** 101954
[45] Cao X R, Tong Z F, Nian Y L, Li J C, Zhou Y N, Zhang Z H, Liu Y X, Gong L, Cheng Z D and He L Q 2025 *Adv. Sci.* **12** 2503024
[46] Lin C H, Ma X Q, Liang K, Xu Y, Yang H Y, Wang J, Ye S, Qiu J M, Song L L, Zhi S Z, Chen J, Zhao P, Duan S C, Wu Z X, Yin L, Wu L Z, Jiang F, Tang Z Q, Cao F, Zhang Q and Mao J 2025 *Nat. Commun.* **16** 7779
[47] Sun X W, Yan Y D, Kang M, Zhao W Y, Yan K F, Wang H, Li R R, Zhao S J, Hua X S, Wang B Y, Zhang W F and Deng Y 2024 *Nat. Commun.* **15** 3870
[48] Yao N Z, Wang H, Wang B, Wang X S and Huang J P 2022 *iScience* **25** 105461
[49] Li Y, Zhu K J, Peng Y G, Li W, Yang T Z, Xu H X, Chen H, Zhu X F and Fan S 2019 *Nat. Mater.* **18** 48
[50] Wang H, Yao N Z, Wang B and Wang X S 2024 *Int. J. Heat Mass Transf.* **221** 125088
[51] Guo J and Qu Z G 2023 *Int. J. Heat Mass Transf.* **212** 124314
[52] Yuan Y, Wang S P, Qian M D and Hou W Y 2025 *iScience* **28** 113547
[53] Zhou Y, Rather L J, Yu K, Yang M, Lu M and Li Q 2024 *Laser Photonics Rev.* **18** 2400530
[54] Hou Y, Liang X S, Li Z Y, Ding Q F, Zhu Z, Sun X L, Li C, Zhou W J, Cao W, Yu Y and Wang Z Y 2025 *Nat. Commun.* **16** 9888